

Table 1: Additional AAST_{EX} symbols

\lesssim	<code>\lessssim, \la</code>	\gtrsim	<code>\gtrsim, \ga</code>
μm	<code>\micron</code>	—	<code>\sbond</code>
\equiv	<code>\dbond</code>	\equiv	<code>\tbond</code>
\odot	<code>\sun</code>	\oplus	<code>\earth</code>
\bigcirc	<code>\diameter</code>		
$^\circ$	<code>\arcdeg, \degr</code>	\square	<code>\sq</code>
$'$	<code>\arcmin</code>	$''$	<code>\arcsec</code>
.d	<code>\fd</code>	.h	<code>\fh</code>
.E	<code>\fm</code>	.s	<code>\fs</code>
.o	<code>\fdg</code>	.!	<code>\farcm</code>
.''	<code>\farcs</code>	.p	<code>\fp</code>
$\frac{1}{2}$	<code>\onehalf</code>	$UBVR$	<code>\ubvr</code>
$\frac{1}{3}$	<code>\onethird</code>	$U-B$	<code>\ub</code>
$\frac{2}{3}$	<code>\twothirds</code>	$B-V$	<code>\bv</code>
$\frac{1}{4}$	<code>\onequarter</code>	$V-R$	<code>\vr</code>
$\frac{3}{4}$	<code>\threequarters</code>	$U-R$	<code>\ur</code>

Table 2: Text-mode accents

\grave{o}	<code>\' {o}</code>	\bar{o}	<code>\={o}</code>	\hat{o}	<code>\t{o}</code>
\acute{o}	<code>\' {o}</code>	\grave{o}	<code>\. {o}</code>	ø	<code>\c{o}</code>
\hat{o}	<code>\^ {o}</code>	ö	<code>\u{o}</code>	ø	<code>\d{o}</code>
\ddot{o}	<code>\" {o}</code>	ö	<code>\v{o}</code>	ø	<code>\b{o}</code>
\tilde{o}	<code>\~ {o}</code>	ö	<code>\H{o}</code>		

Table 3: National symbols

œ	<code>\oe</code>	å	<code>\aa</code>	ł	<code>\l</code>
Œ	<code>\OE</code>	Å	<code>\AA</code>	Ł	<code>\L</code>
æ	<code>\ae</code>	ø	<code>\o</code>	ß	<code>\ss</code>
Æ	<code>\AE</code>	Ø	<code>\O</code>		

Table 4: Math-mode accents

\hat{a}	<code>\hat{a}</code>	\dot{a}	<code>\dot{a}</code>
\check{a}	<code>\check{a}</code>	\ddot{a}	<code>\ddot{a}</code>
\tilde{a}	<code>\tilde{a}</code>	\breve{a}	<code>\breve{a}</code>
\acute{a}	<code>\acute{a}</code>	\bar{a}	<code>\bar{a}</code>
\grave{a}	<code>\grave{a}</code>	\vec{a}	<code>\vec{a}</code>

Table 5: Greek and Hebrew letters (math mode)

α	<code>\alpha</code>	ν	<code>\nu</code>
β	<code>\beta</code>	ξ	<code>\xi</code>
γ	<code>\gamma</code>	\omicron	<code>\o</code>
δ	<code>\delta</code>	π	<code>\pi</code>
ϵ	<code>\epsilon</code>	ρ	<code>\rho</code>
ζ	<code>\zeta</code>	σ	<code>\sigma</code>
η	<code>\eta</code>	τ	<code>\tau</code>
θ	<code>\theta</code>	υ	<code>\upsilon</code>
ι	<code>\iota</code>	ϕ	<code>\phi</code>
κ	<code>\kappa</code>	χ	<code>\chi</code>
λ	<code>\lambda</code>	ψ	<code>\psi</code>
μ	<code>\mu</code>	ω	<code>\omega</code>
\digamma	<code>\digamma</code>	\varkappa	<code>\varkappa</code>
ε	<code>\varepsilon</code>	ς	<code>\varsigma</code>
ϑ	<code>\vartheta</code>	φ	<code>\varphi</code>
ϱ	<code>\varrho</code>		
Γ	<code>\Gamma</code>	Σ	<code>\Sigma</code>
Δ	<code>\Delta</code>	Υ	<code>\Upsilon</code>
Θ	<code>\Theta</code>	Φ	<code>\Phi</code>
Λ	<code>\Lambda</code>	Ψ	<code>\Psi</code>
Ξ	<code>\Xi</code>	Ω	<code>\Omega</code>
Π	<code>\Pi</code>		
\aleph	<code>\aleph</code>	\beth	<code>\beth</code>
\gimel	<code>\gimel</code>	\daleth	<code>\daleth</code>

Table 6: Binary operators (math mode)

\pm	<code>\pm</code>	\cap	<code>\cap</code>
\mp	<code>\mp</code>	\cup	<code>\cup</code>
\setminus	<code>\setminus</code>	\oplus	<code>\oplus</code>
\cdot	<code>\cdot</code>	\sqcap	<code>\sqcap</code>
\times	<code>\times</code>	\sqcup	<code>\sqcup</code>
\ast	<code>\ast</code>	\triangleleft	<code>\triangleleft</code>
\star	<code>\star</code>	\triangleright	<code>\triangleright</code>
\diamond	<code>\diamond</code>	\wr	<code>\wr</code>
\circ	<code>\circ</code>	\bigcirc	<code>\bigcirc</code>
\bullet	<code>\bullet</code>	\bigtriangleup	<code>\bigtriangleup</code>
\div	<code>\div</code>	\bigtriangledown	<code>\bigtriangledown</code>
\triangleleft	<code>\lhd</code>	\triangleright	<code>\rhd</code>
\vee	<code>\vee</code>	\odot	<code>\odot</code>
\wedge	<code>\wedge</code>	\dagger	<code>\dagger</code>
\oplus	<code>\oplus</code>	\ddagger	<code>\ddagger</code>
\ominus	<code>\ominus</code>	\amalg	<code>\amalg</code>
\otimes	<code>\otimes</code>	\unlhd	<code>\unlhd</code>
\oslash	<code>\oslash</code>	\unrhd	<code>\unrhd</code>

Table 7: AMS binary operators (math mode)

†	<code>\dotplus</code>	×	<code>\ltimes</code>
∖	<code>\smallsetminus</code>	⊗	<code>\rtimes</code>
⊍	<code>\Cap, \doublecap</code>	⋈	<code>\leftthreetimes</code>
⊎	<code>\Cup, \doublecup</code>	⋉	<code>\rightthreetimes</code>
⋈	<code>\barwedge</code>	⋊	<code>\curlywedge</code>
∨	<code>\veebar</code>	⋋	<code>\curlyvee</code>
⋈	<code>\doublebarwedge</code>	⊖	<code>\circleddash</code>
⊖	<code>\boxminus</code>	⊗	<code>\circledast</code>
⊗	<code>\boxtimes</code>	⊙	<code>\circledcirc</code>
⊙	<code>\boxdot</code>	⋅	<code>\centerdot</code>
⊕	<code>\boxplus</code>	⋮	<code>\intercal</code>
*	<code>\divideontimes</code>		

Table 8: Miscellaneous symbols

†	<code>\dag</code>	§	<code>\S</code>
©	<code>\copyright</code>	‡	<code>\ddag</code>
¶	<code>\P</code>	£	<code>\pounds</code>
#	<code>\#</code>	\$	<code>\\$</code>
%	<code>\%</code>	&	<code>\&</code>
-	<code>_</code>	{	<code>\{</code>
}	<code>\}</code>		

Table 9: Miscellaneous symbols (math mode)

ℵ	<code>\aleph</code>	/	<code>\prime</code>
ℏ	<code>\hbar</code>	∅	<code>\emptyset</code>
ι	<code>\imath</code>	∇	<code>\nabla</code>
ℵ	<code>\jmath</code>	√	<code>\surd</code>
ℓ	<code>\ell</code>	⊤	<code>\top</code>
∅	<code>\wp</code>	⊥	<code>\bot</code>
ℜ	<code>\Re</code>		<code>\ </code>
ℑ	<code>\Im</code>	∠	<code>\angle</code>
∂	<code>\partial</code>	△	<code>\triangle</code>
∞	<code>\infty</code>	∖	<code>\backslash</code>
□	<code>\Box</code>	◇	<code>\Diamond</code>
∀	<code>\forall</code>	‡	<code>\sharp</code>
∃	<code>\exists</code>	♣	<code>\clubsuit</code>
¬	<code>\neg</code>	◇	<code>\diamondsuit</code>
♭	<code>\flat</code>	♥	<code>\heartsuit</code>
‡	<code>\natural</code>	♠	<code>\spadesuit</code>
℧	<code>\mho</code>		

Table 10: AMS miscellaneous symbols (math mode)

ℏ	<code>\hbar</code>	∖	<code>\backprime</code>
ℏ	<code>\hslash</code>	∅	<code>\varnothing</code>
△	<code>\vartriangle</code>	▲	<code>\blacktriangle</code>
▽	<code>\triangledown</code>	▼	<code>\blacktriangledown</code>
□	<code>\square</code>	■	<code>\blacksquare</code>
◇	<code>\lozenge</code>	◆	<code>\blacklozenge</code>
Ⓢ	<code>\circledS</code>	★	<code>\bigstar</code>
∠	<code>\angle</code>	∠	<code>\sphericalangle</code>
∠	<code>\measuredangle</code>		
∄	<code>\nexists</code>	℄	<code>\complement</code>
℧	<code>\mho</code>	ø	<code>\eth</code>
⊤	<code>\Finv</code>	/	<code>\diagup</code>
∅	<code>\Game</code>	∖	<code>\diagdown</code>
℔	<code>\Bbbk</code>	↑	<code>\restriction</code>

Table 11: Arrows (math mode)

←	<code>\leftarrow</code>	←	<code>\longleftarrow</code>
⇐	<code>\Leftarrow</code>	⇐	<code>\Longleftarrow</code>
→	<code>\rightarrow</code>	→	<code>\longrightarrow</code>
⇒	<code>\Rightarrow</code>	⇒	<code>\Longrightarrow</code>
↔	<code>\leftrightarrow</code>	↔	<code>\longleftrightarrow</code>
⇔	<code>\Leftrightarrow</code>	⇔	<code>\Longleftrightarrow</code>
↦	<code>\mapsto</code>	↦	<code>\longmapsto</code>
↵	<code>\hookleftarrow</code>	↵	<code>\hookrightarrow</code>
↶	<code>\leftharpoonup</code>	↷	<code>\rightharpoonup</code>
↷	<code>\leftharpoondown</code>	↶	<code>\rightharpoondown</code>
⇒	<code>\rightleftharpoons</code>	⇒	<code>\leadsto</code>
↑	<code>\uparrow</code>	⇓	<code>\Updownarrow</code>
⇑	<code>\Uparrow</code>	↗	<code>\nearrow</code>
↓	<code>\downarrow</code>	↘	<code>\searrow</code>
⇓	<code>\Downarrow</code>	↙	<code>\swarrow</code>
⇕	<code>\updownarrow</code>	↖	<code>\nwarrow</code>

Table 12: AMS arrows (math mode)

\dashleftarrow	\dashrightarrow
\leftleftarrows	\rightrightarrows
\leftrightarrows	\rightleftarrows
\Lleftarrow	\Rrightarrow
\twoheadleftarrow	\twoheadrightarrow
\leftarrowtail	\rightarrowtail
\looparrowleft	\looparrowright
\leftrightharpoons	\rightleftharpoons
\curvearrowleft	\curvearrowright
\circlearrowleft	\circlearrowright
\Lsh	\Rsh
\upuparrows	\downdownarrows
\upharpoonleft	\upharpoonright
\downharpoonleft	\downharpoonright
\multimap	\rightsquigarrow
\leftrightsquigarrow	
\nleftarrow	\nrightarrow
\nLeftarrow	\nRightarrow
\nleftrightarrow	\nLeftrightarrow

Table 13: Relations (math mode)

\leq	\geq
\prec	\succ
\preceq	\succeq
\ll	\gg
\subset	\supset
\subseteq	\supseteq
\sqsubset	\sqsupset
\sqsubseteq	\sqsupseteq
\in	\ni
\vdash	\dashv
\smile	\mid
\frown	\parallel
\neq	\perp
\equiv	\cong
\sim	\bowtie
\simeq	\propto
\asymp	\models
\approx	\doteq
	\Join

Table 14: AMS binary relations (math mode)

\leqq	\geqq
\leqslant	\geqslant
\leqslantless	\leqslantgtr
\lesssim	\gtrsim
\lessapprox	\gtrapprox
\approxeq	\eqsim
\lessdot	\gtrdot
\lll, \llless	\ggg, \gggtr
\lessgtr	\gtrless
\lesseqgtr	\gtreqless
\lesseqqgtr	\gtreqqless
\doteqdot, \Doteq	\eqcirc
\risingdotseq	\circeq
\fallingdotseq	\triangleq
\backsim	\thicksim
\backsimeq	\thickapprox
\subseteqq	\supseteqq
\Subset	\Supset
\sqsubset	\sqsupset
\preccurlyeq	\succcurlyeq
\curlyeqprec	\curlyeqsucc
\precsim	\succsim
\precapprox	\succapprox
\vartriangleleft	\vartriangleright
\trianglelefteq	\trianglerighteq
\Vdash	\Vdash
\Vvdash	
\smallsmile	\shortmid
\smallfrown	\shortparallel
\bumpeq	\between
\Bumpeq	\pitchfork
\varpropto	\backepsilon
\blacktriangleleft	\blacktriangleright
\therefore	\because

Table 15: AMS negated relations (math mode)

\nless	\ngtr
\nleq	\ngeq
\nleqslant	\ngeqslant
\nleqq	\ngeqq
\lneq	\gneq
\lneqq	\gneqq
\lvertneqq	\gvertneqq
\lnsim	\gnsim
\lnapprox	\gnapprox
\nprec	\nsucc
\npreceq	\nsucceq
\precneqq	\succneqq
\precnsim	\succnsim
\precnapprox	\succnapprox
\nsim	\ncong
\nshortmid	\nshortparallel
\nmid	\nparallel
\nvDash	\nvDash
\nVDash	\nVDash
\ntriangleleft	\ntriangleright
\ntrianglelefteq	\ntrianglerighteq
\nsubseteq	\nsupseteq
\nsubseteqq	\nsupseteqq
\subsetneq	\supsetneq
\varsubsetneq	\varsupsetneq
\subseteqq	\supseteqq
\varsubseteqq	\varsupseteqq

Table 17: Delimiters (math mode)

(())
[[]]
{	{	}	}
[\lfloor]	\rfloor
[\lceil]	\rceil
<	\langle	>	\rangle
/	/	\	\backslash
	\vert		\Vert
↑	\uparrow	↑	\Uparrow
↓	\downarrow	↓	\Downarrow
↕	\updownarrow	↕	\Updownarrow
┌	\ulcorner	┐	\urcorner
└	\llcorner	┘	\lrcorner

Table 16: Variable-sized symbols (math mode)

\sum	\sum	\sum	\bigcap	\bigcap	\bigcap	\bigcap
\prod	\prod	\prod	\bigcup	\bigcup	\bigcup	\bigcup
\coprod	\coprod	\coprod	\bigsqcup	\bigsqcup	\bigsqcup	\bigsqcup
\int	\int	\int	\bigvee	\bigvee	\bigvee	\bigvee
\oint	\oint	\oint	\bigwedge	\bigwedge	\bigwedge	\bigwedge
\odot	\odot	\odot	\bigotimes	\bigotimes	\bigotimes	\bigotimes
\oplus	\oplus	\oplus	\bigoplus	\bigoplus	\bigoplus	\bigoplus

Table 18: Function names (math mode)

\arccos	\csc	\ker	\min
\arcsin	\deg	\lg	\Pr
\arctan	\det	\lim	\sec
\arg	\dim	\liminf	\sin
\cos	\exp	\limsup	\sinh
\cosh	\gcd	\ln	\sup
\cot	\hom	\log	\tan
\coth	\inf	\max	\tanh

DETECTION OF VHE RADIATION FROM THE BL LAC PG 1553+113 WITH THE MAGIC TELESCOPE

J. ALBERT^A, E. ALIU^B, H. ANDERHUB^C, P. ANTORANZ^D, A. ARMADA^B, C. BAIXERAS^E, J. A. BARRIO^D, H. BARTKO^G, D. BASTIERI^H, J. BECKER^F, W. BEDNAREK^I, K. BERGER^A, C. BIGONGIARI^H, A. BILAND^C, R. K. BOCK^{G,H}, P. BORDAS^S, V. BOSCH-RAMON^S, T. BRETZ^A, I. BRITVITCH^C, M. CAMARA^D, E. CARMONA^G, A. CHILINGARIAN^K, S. CIPRINI^L, J. A. COARASA^G, S. COMMICHAU^C, J. L. CONTRERAS^D, J. CORTINA^B, V. CURTEF^F, V. DANIELYAN^K, F. DAZZI^H, A. DE ANGELIS^I, R. DE LOS REYES^D, B. DE LOTTO^I, E. DOMINGO-SANTAMARÍA^B, D. DORNER^A, M. DORO^H, M. ERRANDO^B, M. FAGIOLINI^O, D. FERENC^N, E. FERNÁNDEZ^B, R. FIRPO^B, J. FLIX^B, M. V. FONSECA^D, L. FONT^E, M. FUCHS^G, N. GALANTE^M, M. GARCZARCZYK^G, M. GAUGH^H, M. GILLER^J, F. GOEBEL^G, D. HAKOBYAN^K, M. HAYASHIDA^G, T. HENGSTEBECK^M, D. HÖHNE^A, J. HOSE^G, C. C. HSU^G, P. JACON^J, T. JOGLER^G, O. KALEKIN^M, R. KOSYRA^G, D. KRANICH^C, R. KRITZER^A, A. LAILLE^N, P. LIEBING^G, E. LINDFORS^L, S. LOMBARDI^H, F. LONGO^I, J. LÓPEZ^B, M. LÓPEZ^D, E. LORENZ^{C,G}, P. MAJUMDAR^G, G. MANEVA^P, K. MANNHEIM^A, O. MANSUTTI^I, M. MARIOTTI^H, M. MARTÍNEZ^B, D. MAZIN^G, C. MERCK^G, M. MEUCCI^O, M. MEYER^A, J. M. MIRANDA^D, R. MIRZOYAN^G, S. MIZOBUCHI^G, A. MORALEJO^B, K. NILSSON^L, J. NINKOVIC^G, E. OÑA-WILHELM^B, N. OTTE^G, I. OYA^D, D. PANEQUE^G, R. PAOLETTI^O, J. M. PAREDES^S, M. PASANEN^L, D. PASCOLI^H, F. PAUSS^C, R. PEGNA^O, M. PERSIC^{I,Q}, L. PERUZZO^H, A. PICCIOLI^O, M. POLLER^A, N. PUCHADES^B, E. PRANDINI^H, A. RAYMERS^K, W. RHODE^F, M. RIBÓ^S, J. RICO^B, M. RISSI^C, A. ROBERT^E, S. RÜGAMER^A, A. SAGGION^H, A. SÁNCHEZ^E, P. SARTORI^H, V. SCALZOTTO^H, V. SCAPIN^H, R. SCHMITT^A, T. SCHWEIZER^G, M. SHAYDUK^{M,G}, K. SHINOZAKI^G, N. SIDRO^B, A. SILLANPÄÄ^L, D. SOB CZYNSKA^J, A. STAMERRA^O, L. S. STARK^C, L. TAKALO^L, P. TEMNIKOV^P, D. TESCARO^B, M. TESHIMA^G, N. TONELLO^G, D. F. TORRES^B, N. TURINI^O, H. VANKOV^P, V. VITALE^I, R. M. WAGNER^G, T. WIBIG^J, W. WITTEK^G, R. ZANIN^H, J. ZAPATERO^E

Draft version December 2, 2024

ABSTRACT

In 2005 and 2006, the MAGIC telescope has observed very high energy gamma-ray emission from the distant BL Lac object PG 1553+113. The overall significance of the signal is 8.8σ for 18.8 h observation time. The light curve shows no significant flux variations on a daily time-scale, the flux level during 2005 was, however, significantly higher compared to 2006. The differential energy spectrum between ~ 90 GeV and 500 GeV is well described by a power law with photon index $\Gamma = 4.2 \pm 0.3$. The combined 2005 and 2006 energy spectrum provides an upper limit of $z = 0.74$ on the redshift of the object.

Subject headings: PG 1553+113, BL Lac, AGN, VHE gamma-ray, imaging air Cherenkov telescope

1. INTRODUCTION

1.1. The BL Lac object PG 1553+113

The Active Galactic Nucleus (AGN) PG 1553+113 was first reported in the Palomar-Green catalogue of UV bright objects (Green et al. 1986). It was the only new BL Lac object found in the survey and the first BL Lac object found in an optical survey. Its spectrum is,

typical for BL Lac objects, featureless (Miller & Green 1983) and the optical variability strong ($m_p = 13.2 - 15.0$; Miller et al. (1988)). The spectral characteristics are close to those of X-ray selected BL Lacs (Falomo & Treves 1990) and it is classified in the literature as intermediate BL Lac (Laurent-Muehleisen et al. 1999; Nieppola et al. 2006) or high-frequency peaked BL Lac (Giommi et al. 1995), as its synchrotron peak frequency lies on the borderline of these two groups.

Despite several attempts, no emission or absorption lines have been found in the spectrum of PG 1553+113 (Falomo & Treves 1990). Thus only indirect methods can be used to determine the redshift z (e.g. Sbarufatti et al. (2005, 2006)). The host galaxy was not resolved in Hubble Space Telescope (HST) images (Urry et al. 2000), it is therefore safe to assume $z > 0.25$. The observation of very high energy (VHE, defined here as $E \gtrsim 100$ GeV) γ -ray emission, on the other hand, may permit to set an upper limit on z . The γ -ray absorption in the Extragalactic Background Light (EBL) by means of $e^+ e^-$ pair production (Stecker et al. 1992; Aharonian et al. 2006a) can significantly affect the shape of the observed energy spectrum depending on the source redshift. Based on present-day EBL models and the observed γ -ray spectrum, one can derive the intrinsic spectrum as a function of z . Physical constraints on e.g. the slope of the intrinsic spectrum may then permit to set upper limits on the possible redshift (Aharonian et al. 2006b).

^a Universität Würzburg, D-97074 Würzburg, Germany

^b Institut de Física d'Altes Energies, Edifici Cn., E-08193 Bellaterra (Barcelona), Spain

^c ETH Zurich, CH-8093 Switzerland

^d Universidad Complutense, E-28040 Madrid, Spain

^e Universitat Autònoma de Barcelona, E-08193 Bellaterra, Spain

^f Universität Dortmund, D-44227 Dortmund, Germany

^g Max-Planck-Institut für Physik, D-80805 München, Germany

^h Università di Padova and INFN, I-35131 Padova, Italy

ⁱ Università di Udine, and INFN Trieste, I-33100 Udine, Italy

^j University of Łódź, PL-90236 Lodz, Poland

^k Yerevan Physics Institute, AM-375036 Yerevan, Armenia

^l Tuorla Observatory, Turku University, FI-21500 Piikkiö, Finland

^m Humboldt-Universität zu Berlin, D-12489 Berlin, Germany

ⁿ University of California, Davis, CA-95616-8677, USA

^o Università di Siena, and INFN Pisa, I-53100 Siena, Italy

^p Institute for Nuclear Research and Nuclear Energy, BG-1784 Sofia, Bulgaria

^q INFN/Osservatorio Astronomico and INFN Trieste, I-34131 Trieste, Italy

^r Università di Pisa, and INFN Pisa, I-56126 Pisa, Italy

^s Universitat de Barcelona, E-08028 Barcelona, Spain

* correspondence: D. Kranich: kranich@physics.ucdavis.edu, R. Wagner: rwagner@mppmu.mpg.de

PG 1553+113 belongs to a catalog of X-ray bright objects (Donato et al. 2005) and, based on its Spectral Energy Distribution (SED) properties, was one of the most promising candidates from a list of VHE γ -ray emitting candidates proposed by Costamante & Ghisellini (2002). So far, upper limits on the γ -ray emission have been reported by the Whipple collaboration (19% Crab flux above 390 GeV, de la Calle Perez et al. (2003)) and Milagro (Williams 2004). Recently the H.E.S.S. collaboration has presented evidence for a γ -ray signal at the 4σ level (up to 5.3σ using a low energy threshold analysis) above 200 GeV corresponding to about 2% of the Crab flux (Aharonian et al. 2006b). The energy spectrum was found to have a steep slope with $\Gamma = 4.0 \pm 0.6_{stat}$ and an upper limit on the redshift of $z < 0.74$ was derived.

1.2. The MAGIC telescope

The MAGIC telescope is located on the Canary Island of La Palma (28.75° N, 17.86° W, at 2225 m asl.). The telescope comprises a 17 m diameter tessellated, parabolic mirror with a total surface of 234 m^2 , a light-weight space-frame made from carbon fiber-epoxy tubes, and a camera with 576 hemispherical photomultiplier tubes (PMT) with enhanced quantum efficiency (Paneque et al. 2004). The field of view of the camera is 3.5° while the trigger area covers about 2.0° in diameter. The fast PMT analog signals are routed via optical fibers to the DAQ-system electronics in the counting house 80 m away. The signals are digitized by dual range 300 MHz FADCs. MAGIC can explore γ -rays at energies down to 50 GeV (trigger threshold, depending on the zenith angle), critical for the observation of medium redshift VHE sources with steeply falling spectra like PG 1553+113. The MAGIC telescope parameters and performance are described in more detail in Baixeras et al. (2004) and Cortina et al. (2005). Simultaneous with MAGIC, optical observations were performed with the KVA telescope on La Palma, operated remotely from Tuorla Observatory. The main instrument is a 60 cm (f/15) Cassegrain telescope equipped with a CCD capable of polarimetric measurements. A 35 cm auxiliary telescope (f/11) is mounted on the same RA axis. This telescope is used for BVRI CCD photometry.

2. OBSERVATION AND DATA ANALYSIS

PG 1553+113 was observed with the MAGIC telescope for 8.9 h in April and May 2005, i.e. at about the same time when also H.E.S.S. observed the source, and for 19 h from January to April 2006. In addition to the observations with MAGIC and the 35 cm photometric telescope simultaneous data in X-rays were taken with the All-Sky-Monitor on board the RXTE satellite. These data are provided on the web at http://heasarc.gsfc.nasa.gov/xte_weather/. Data taken during non-optimal weather conditions or affected by hardware problems were excluded from the analysis. Also, only data taken at small zenith angles $ZA < 30^\circ$ (corresponding to a low energy threshold which is suitable for a steep energy spectrum) were retained although measurements went up to 53° . After these selection cuts, 7.0 h and 11.8 h of good data remained for 2005 and 2006, respectively. Given the mean ZA of $\sim 22^\circ$ γ -ray events above ~ 90 GeV have been

used for the physics analysis.

In addition to the so-called on-data from PG 1553+113, off-data were taken on a nearby sky position where no γ -ray source is expected, but with comparable zenith angle distribution and night sky background light conditions. The off-data are used to determine the background content in the signal region of the on-data. This was done by means of a second order polynomial fit (without linear term) to the ALPHA distribution of the normalized off-data. The normalization was done in the ALPHA region between 30° and 90° where no γ -ray events are expected. The ALPHA parameter describes the orientation of a shower image in the camera with respect to the camera center. Air showers which are aligned parallel to the telescope axis do have ALPHA values close to zero. In total, 14.5 h of off-data (6.5 h from 2005 and 8.0 h from 2006) have been used for the analysis. Since the two off-samples were in good agreement we used the combined data to analyze the individual on-data samples.

The data were analyzed using the standard MAGIC analysis programs for calibration, image cleaning, cut optimization and energy reconstruction (Bretz et al. 2005; Gaug et al. 2005; Wagner et al. 2005). The primary method for discrimination between hadron- and γ -ray-induced showers is based on the Random Forest (RF) method (Breiman 2001; Bock et al. 2004) which was trained on off-data and Monte Carlo (MC) generated γ -ray events. The significance of any excess was calculated according to Eq. 17 in Li & Ma (1983) where the on to off ratio α was derived, taking into account the smaller error from the off-data fit. In addition to the cut optimization, the RF method was also used for the energy estimation based on the image parameters of a statistically independent MC γ -ray sample. The average energy resolution obtained was 24% RMS. All MC data used in this analysis were generated using the CORSIKA version 6.019 (Knapp & Heck 2004; Majumdar et al. 2005).

3. RESULTS

Combining the data from 2005 and 2006, a very clear signal is seen in the image parameter ALPHA, as shown in Fig. 1. Defining the signal region as $ALPHA < 12^\circ$ (containing about 90% of the γ -ray events), an excess of 1032 over 8730 background events yields a total significance of 8.8σ . The individual results for the years 2005 and 2006 are listed separately in Table 1. In both years the object has been clearly detected with a significance $> 6\sigma$.

The γ -ray, X-ray and optical light curve of PG 1553+113 are shown in Fig. 2. While the optical data shows significant short term variability on the 25% level the X-ray data is consistent with a constant emission, given the weighted mean of 0.15 ± 0.03 counts/s. In γ -rays there is no evidence for short term variability, but a significant change in the flux level from 2005 to 2006 is found, given a systematic error of the analysis on the flux level of about 30%. The average integral flux between 120 GeV and 400 GeV is given as $F = 10.0 \pm 0.23_{stat}$ and $F = 3.7 \pm 0.08_{stat}$ (with F given in units of $10^{-11}\text{ cm}^{-2}\text{ s}^{-1}$) for 2005 and 2006, respectively. On February 25th, prior to the optical flare, the optical polarimetry of the source was measured with the KVA 60 cm telescope. The degree of optical linear polarisation was $8.3 \pm 0.2\%$ and the polarisation position

angle was $139.1^\circ \pm 0.4^\circ$. It should be noted, that since the host galaxy can not be resolved for this object, the optical flux should correspond to the emission from the AGN core.

The combined 2005 and 2006 differential energy spectrum for PG 1553+113 is shown in Fig. 3. The integral fluxes above 200 GeV and the spectral slope coefficients for the different samples are listed in Tab. 1. Effects on the spectrum determination introduced by the limited energy resolution were corrected by 'unfolding' according to Mizobuchi et al. (2005). For comparison, the MAGIC Crab energy spectrum and the H.E.S.S. PG 1553+113 energy spectrum (Aharonian et al. 2006b) are also shown. The energy spectrum is well described by a pure power law:

$$\frac{dN}{dE} = (1.8 \pm 0.3_{stat}) \cdot \left(\frac{E}{200 \text{ GeV}} \right)^{-4.2 \pm 0.3_{stat}} \quad (1)$$

(in units of $10^{-10} \text{ cm}^{-2} \text{ s}^{-1} \text{ TeV}^{-1}$, $\chi^2/NDF = 1.5/4$). Compared to the Crab spectrum in the same energy range ($\Gamma = 2.41 \pm 0.05$; Wagner et al. (2005)) this spectrum is significantly steeper. The spectral slopes of the individual years are in good agreement although the flux level above 200 GeV is about a factor 3 larger in 2005 compared to 2006. This is also shown in the light curve. The estimated systematic error on the analysis (signal extraction, cut efficiencies etc.) is 25% (dark colored band in the figure) and 30% on the energy scale (light colored band).

4. DISCUSSION

The BL Lac object PG 1553+113 has been detected at 8.8σ with the MAGIC telescope in 18.8 hours of observation during 2005 and 2006. This confirms the tentative signal seen by H.E.S.S. at a higher energy threshold with data taken at about the same time as MAGIC in the 2005 period (Aharonian et al. 2006b). The source, therefore, can now be considered as firmly detected.

The agreement between the measured H.E.S.S. and MAGIC energy spectra of PG 1553+113 in 2005 is reasonably good. While the spectral slope is consistent within errors, the absolute flux above 200 GeV in 2005 is by a factor 4 larger compared to H.E.S.S. This difference may in part be explained by the systematic errors of both measurements but also by variations in the flux level of the source (the observations with H.E.S.S. were commenced after MAGIC). The observed energy spectrum is steeper than that of any other known BL Lac object. This may be an indication of a large redshift ($z \gtrsim 0.3$), but can as well be attributed to intrinsic absorption at the AGN or, more naturally, to an inverse Compton peak position at lower energies. The spectrum can, however, be used to derive an upper limit on the source redshift from physical constraints on the intrinsic photon index ($\Gamma_{int} > 1.5$) as discussed in Aharonian et al. (2006b). Using the lower limit on the evolving EBL density from Kneiske et al. (2004) we derived a 2σ upper limit on the redshift of $z < 0.74$. The same value was reported by Aharonian et al. (2006b) where a slightly different EBL model was used.

The Broad band SED of PG 1553+113 together with the results from a model calculation are shown in Fig. 4. The VHE data points correspond to the intrinsic spectrum of PG 1553+113 as derived for a redshift of $z = 0.3$. The black points at low energies denote the average optical and X-ray flux taken at the same time as the MAGIC observations. The gray hatched radio, optical and X-ray non-simultaneous data were taken from Giommi et al. (2002). The solid line shows the result of a model fit to the simultaneously recorded data (black points) using a homogeneous, one-zone Synchrotron Self-Compton (SSC) model as provided by Krawczynski et al. (2004). As can be seen from Fig. 4, the γ -ray, X-ray and optical data are well described by the model. This is not the case for the radio data where intrinsic absorption requires a much larger emitting volume compared to X-rays and γ -rays. Except for a somewhat smaller radius of the emitting region, identical model parameters as in Costamante & Ghisellini (2002) have been used: Doppler factor $D = 21$, magnetic field strength $B = 0.7 \text{ G}$, radius of the emitting region $R = 1.16^{+0.62}_{-0.21} \cdot 10^{16} \text{ cm}$, electron energy density $\rho_e = 0.11^{+0.18}_{-0.06} \text{ erg/cm}^3$ slope of the electron distribution $\alpha_e = -2.6$ for $8.2 < \log(E/\text{eV}) < 9.8^{+0.2}_{-0.05}$ and $\alpha_e = -3.6$ for $9.8^{+0.2}_{-0.05} < \log(E/\text{eV}) < 10.6^{+1.6}_{-0.0}$. The limits on some of these parameters indicate the change of the SED model parameters when varying the assumed redshift from $z=0.2$ up to $z=0.7$ (parameters without limits were kept constant for all fits). In the case of $z \geq 0.56$ the SED model can not accurately describe the data and, based on the obtained χ^2 value, a redshift of 0.56 is excluded on the 4.5σ level. For a comparison of the model parameters with those from other BL Lacs we refer to Costamante & Ghisellini (2002).

PG 1553+113 was in a high state in the optical in both years showing a strong flare at the end of March 2006. The high linear polarization of the optical emission ($8.3 \pm 0.2\%$) indicates that a sizeable fraction of the optical flux is indeed synchrotron radiation. In γ -rays only a significant change in the flux level from 2005 to 2006 is found while there is no evidence for variability in X-rays. As a result, a possible correlation between the different energy bands can not be established. A possible connection between the γ -ray detection and the optical high state can, however, not be excluded. The optical flare without X-ray or γ -ray counterpart may still be explained by external-inverse-Compton (EIC) models which predict a time lag of the X-rays and γ -rays with respect to the optical emission.

ACKNOWLEDGMENTS

We would like to thank the IAC for the excellent working conditions on the La Palma Observatory Roque de los Muchachos. We are grateful to the ASM/RXTE team for their quick-look results. The support of the German BMBF and MPG, the Italian INFN and the Spanish CI-CYT is gratefully acknowledged. This work was also supported by ETH Research Grant TH-34/04-3 and by Polish Grant MNiI 1P03D01028.

REFERENCES

- Aharonian, F. *et al.* 2006a, *Nature*, **440**, 1018
 Aharonian, F. *et al.* 2006b *A&A*, **448**, L19
 Baixeras, C. *et al.* 2004, *Nucl.Inst.Meth.*, **A 518**, 188
 Bock, R. K. *et al.* 2004, *Nucl.Inst.Meth.*, **A 516**, 511
 Breiman, L. 2001, *Machine Learning*, **45**, 5
 Bretz, T. *et al.* 2005, AIP Conference Proceedings, **745**, 730
 Costamante L. & Ghisellini, G. 2002, *A&A*, **384**, 56
 Cortina, J. *et al.* 2005, Proc. 29th ICRC, Pune, 5-359, preprint (astro-ph/0508274)
 de la Calle Perez, I. *et al.* 2003, *ApJ*, **599**, 909
 Donato, D., Sambruna, R. M., & Gliozzi, M. 2005, *A&A*, **433**, 1163
 Falomo, R. & Treves, A. 1990, *PASP*, **102**, 1120
 Gaug, M. *et al.* 2005, Proc. 29th ICRC, Pune, 5-375, preprint (astro-ph/0508274)
 Giommi, P., Ansari, S. G., & Micol, A. 1995, *A&AS*, **109**, 267
 Giommi, P., Massaro, E., & Palumbo, G. 2002, Proc. Blazar Astrophysics with BeppoSAX and other Observatories, 2002, 63-100
 Green, R. F., Schmidt, M., & Liebert, J. 1986, *ApJS*, **61**, 305
 Knapp, J. & Heck, D. 2004, EAS Simulation with CORSIKA: A Users manual
 Kneiske, T. M., Bretz, T., Mannheim, K., & Hartmann, D. H. 2004, *A&A*, **413**, 807
 Krawczynski, H. *et al.* 2004, *ApJ*, **601**, 151
 Laurent-Muehleisen, S. A., Kollgaard, R. I., Feigelson, E. D., Brinkmann, W., & Siebert, J. 1999, *ApJ*, **525**, 127
 Li, T. & Ma, Y. 1983, *ApJ* **272**, 317
 Majumdar, P. *et al.* 2005, Proc. 29th ICRC, Pune, 5-203, preprint (astro-ph/0508274)
 Miller, H. R., Carini, M. T., Gaston, B. J., & Hutter, D. J. 1988, Proc. of the IUE Symposium (Greenbelt), 303
 Miller, H. R. & Green, R. F. 1983, *BAAS*, **15**, 957
 Mizobuchi, S. *et al.* 2005, Proc. 29th ICRC, Pune, 5-323, preprint (astro-ph/0508274)
 Nieppola, E., Tornikoski, M., & Valtaoja, E. 2006, *A&A*, **445**, 441
 Paneque, D., Gebauer, H. J., Lorenz, E., & Mirzoyan, R. 2004, *Nucl.Inst.Meth.*, **A 518** 619
 Primack, J., Bullock, J. S., & Somerville, R. S. 2005, AIP Conference Proceedings, **745**, 23
 Sbarufatti, B., Treves, A., & Falomo, R. 2005, *ApJ*, **635**, 173
 Sbarufatti, B., Treves, A., Falomo, R., Heidt, J., Kotilainen, J., & Scarpa, R. 2006, *AJ*, 132, 1
 Stecker, F. W., de Jager, O. C., & Salamon, M. H. 1992, *ApJ* **390**, 49
 Urry, C. M., Scarpa, R., O'Dowd, M., Falomo, R., Pesce, J. E. & Treves, A. 2000, *ApJ*, **532**, 816
 Wagner, R. M. *et al.* 2005, Proc. 29th ICRC, Pune, 4-163, preprint (astro-ph/0508244)
 Williams, D. 2004, AIP Conference Proceedings, **745**, 499

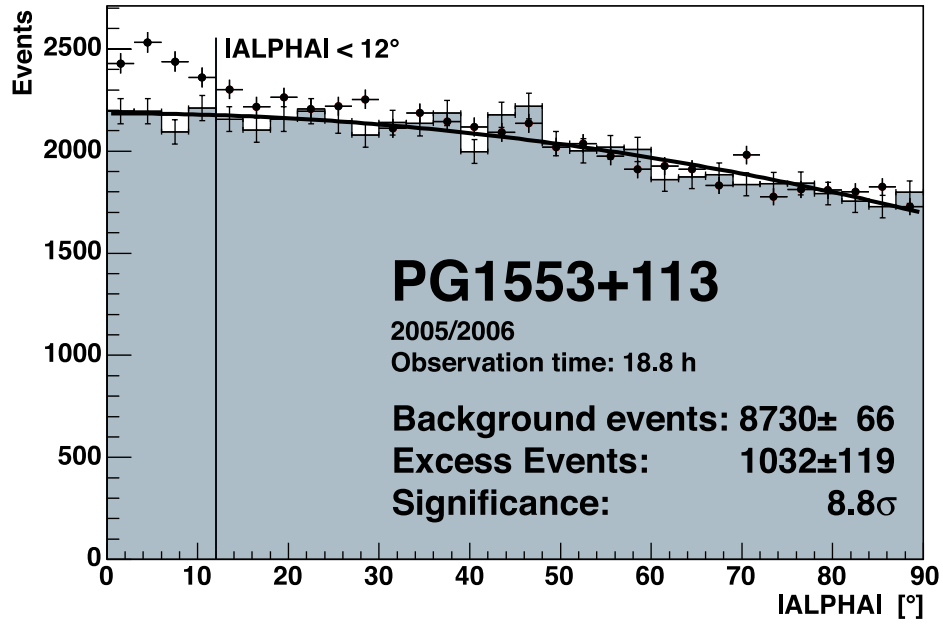


FIG. 1.— ALPHA plot for the combined 2005 and 2006 PG 1553+113 data after cuts. The diagram also shows the distribution of the (normalized) off-data and a second-order polynomial describing the off-data.

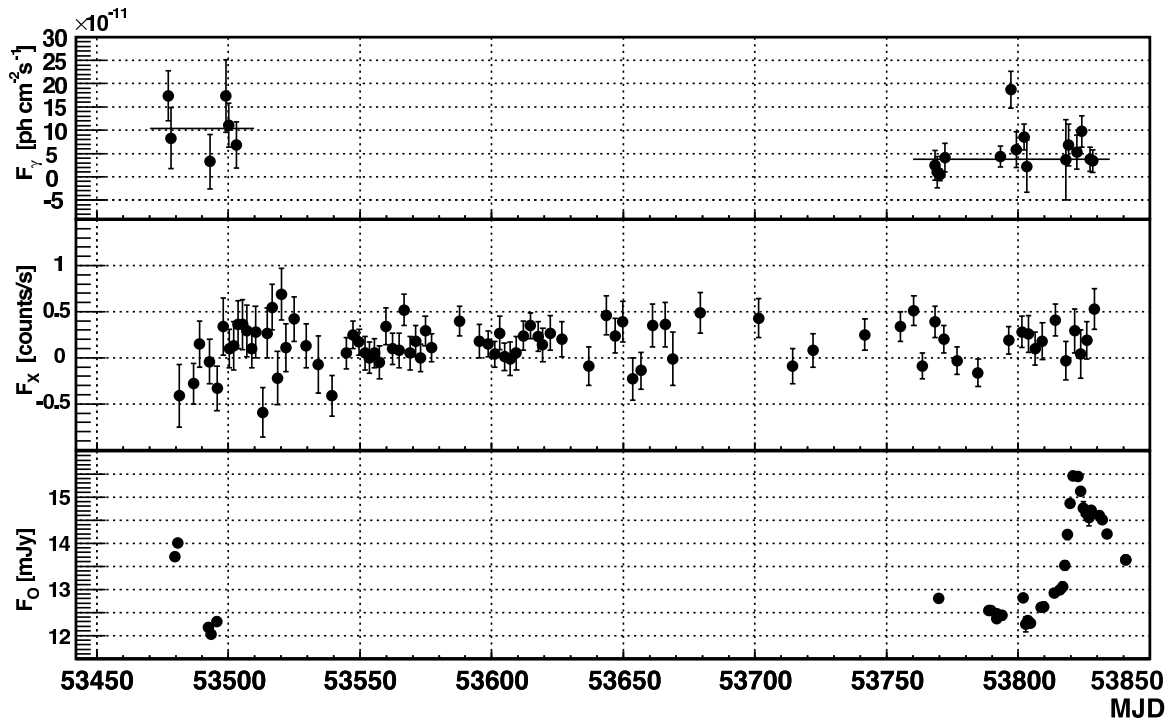


FIG. 2.— VHE γ -ray (120 GeV – 400 GeV), X-ray (2 keV – 10 keV) and optical light curve (R-Band) of PG 1553+113 in 2005 and 2006. The horizontal bars in the top panel correspond to the average flux during 2005 and 2006, respectively.

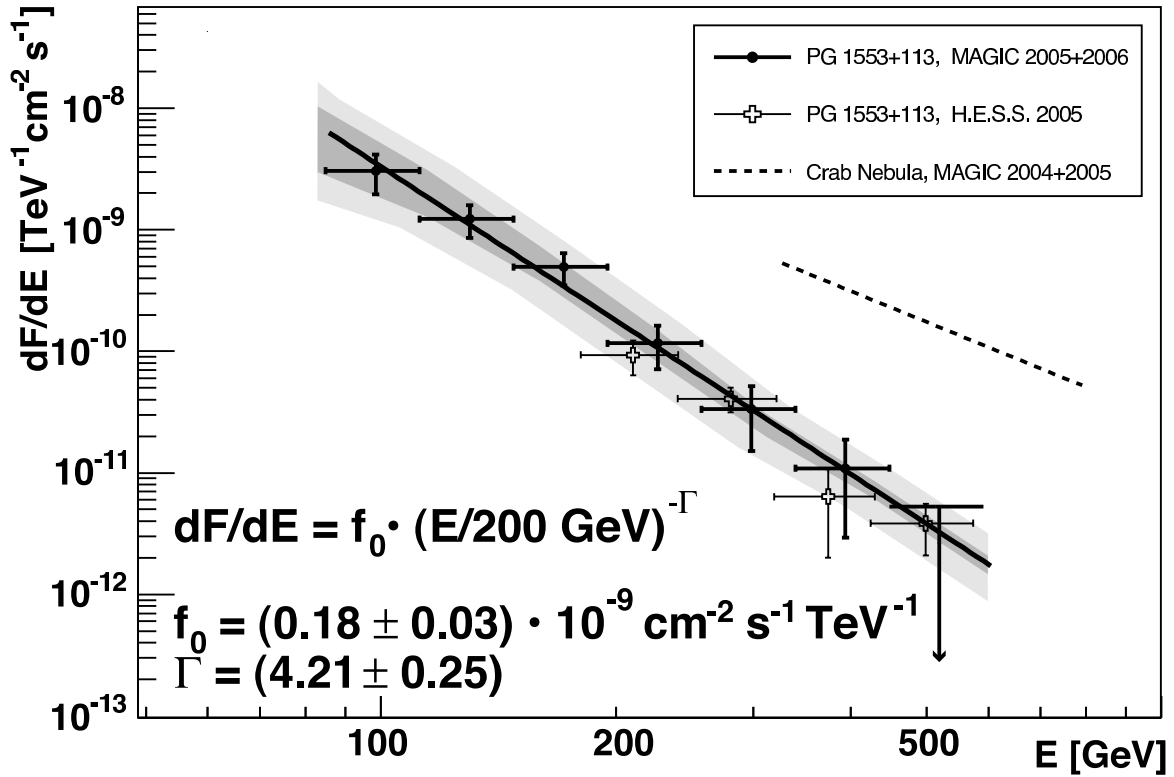


FIG. 3.— Differential energy spectrum of PG 1553+113 as derived from the combined 2005 and 2006 data. The MAGIC Crab energy spectrum and the H.E.S.S. PG 1553+113 energy spectrum have been included for comparison.

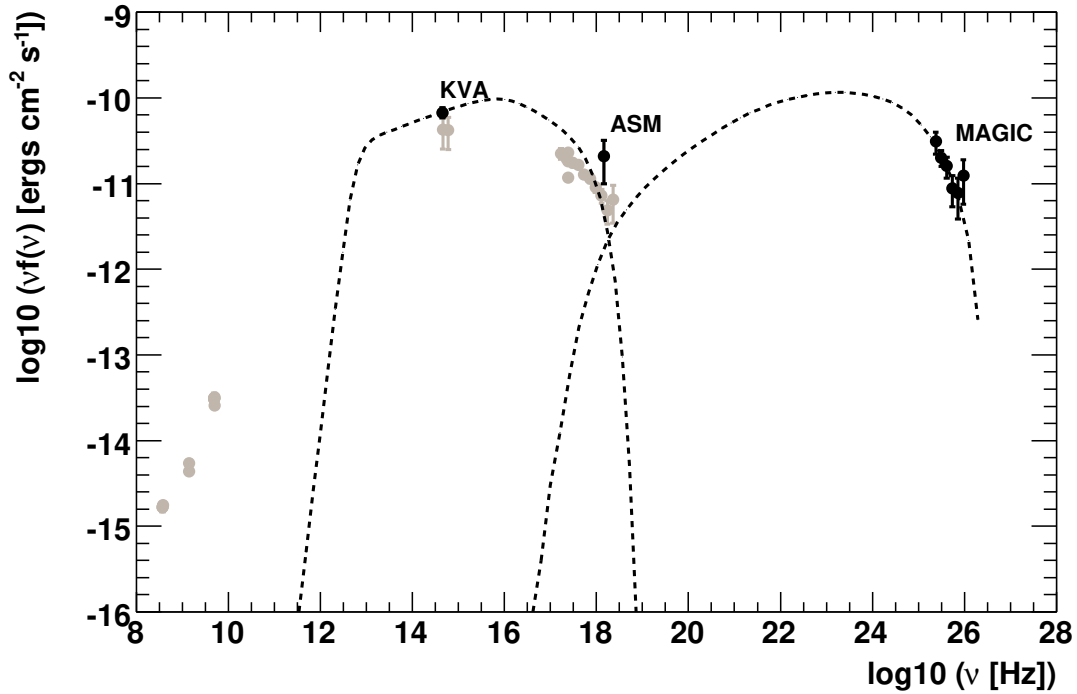


FIG. 4.— Broad band SED of PG 1553+113. The solid lines are the result of a SSC model fit to the black data points using the code provided by Krawczynski et al. (2004) (see text). The gray points comprise non-simultaneous radio, optical and X-ray data from Giommi et al. (2002).

TABLE 1
RESULTS FROM THE PG 1553+113 ANALYSIS AS DERIVED FOR 2005 AND 2006.

Year	on time	N_{on}	N_{off}	N_{excess}	on / off	sigma	$F(E > 200\text{GeV})^a$	photon index
2005	7.0 h	3944	3501 ± 26	443 ± 68	0.20	6.7σ	$2.0 \pm 0.6_{stat} \pm 0.6_{sys}$	4.31 ± 0.45
2006	11.8 h	5815	5228 ± 39	588 ± 86	0.30	7.0σ	$0.6 \pm 0.2_{stat} \pm 0.2_{sys}$	3.95 ± 0.23
2005+2006	18.8 h	9761	8730 ± 66	1032 ± 119	0.49	8.8σ	$1.0 \pm 0.4_{stat} \pm 0.3_{sys}$	4.21 ± 0.25

^a integral flux in units of $10^{-11} \text{ cm}^{-2} \text{ s}^{-1}$